Hydrocarbon generation and expulsion of the Fengcheng Formation in the Mahu sag, Junggar Basin, China: Implications for shale oil resource potential

Yuping Wu[1], Chenglin Liu[2], Fujie Jiang[2], Tao Hu[2], Chenxi Zhang[2], Jiahao Lv[2], Meiling Hu[2], Renda Huang[2], Guanyun Wu[2], and Rizwan Sarwar Awan[3]

Abstract

The Permian source rocks in the Junggar Basin are widely developed, especially the Fengcheng Formation, which is the most significant source rock in the basin. However, due to insufficient research on the hydrocarbon generation (HG) and hydrocarbon expulsion (HE) characteristics of the source rocks, it is unclear whether a significant amount of retained hydrocarbons remain within shales. In general, the original organic matter abundance and kerogen type control hydrocarbon generation potential (HGP) and HE capacity in lacustrine shales. Therefore, the degradation rate method was used to establish the original organic carbon recovery model for different types of kerogen. Combined with the geologic and geochemical characteristics of the source rock, the HG, HE, and shale oil resource potential of the Fengcheng shale have been evaluated. We have found that the Fengcheng shale is mainly carbonate-type mudstone widely distributed with an average thickness greater than 100 m. The Fengcheng shale is composed of type II kerogen and reached the mature to high-mature thermal maturity stage, with the maximum original organic carbon exceeding 4.0 wt%. Meanwhile, the amount of retained hydrocarbons within shales is abundant according to the HGP model. Monte Carlo simulation finds that the shale oil resources of the Fengcheng shale are 23.30×10^8 t. Free oil resources account for 60%, reaching 13.75×10^8 t, indicating tremendous shale oil exploration potential.

Introduction

Global energy demand is continuously rising, and unconventional oil resources have become a key target for petroleum exploration. According to previous works, shale oil resources are abundant in the world (Wendebourg et al., 2017). Unlike conventional petroleum, shale oil is the self-sourced and self-retained hydrocarbons in lacustrine shales (Li et al., 2019; Jin et al., 2022). These shales are characterized by ultralow porosity and permeability. Thus, only after hydraulic fracturing stimulation can the oil in shale reservoirs be better recovered (Jin et al., 2022). At present, most of the production of shale oil comes from marine formations. Furthermore, the successful exploitation of shale oil in America and Canada has brought lacustrine shales into focus. Compared with marine shales, the lacustrine shale systems have the unique characteristics of a limited target area, strong heterogeneity, low to moderate maturity, and high clay mineral content (Katz and Lin, 2014; Liang et al., 2017; Hu et al., 2018, 2022a; Li et al., 2019). However, previous studies have shown that the thicknesses of lacustrine shales often are significantly greater than marine shales (Katz and Lin, 2014). Therefore, there may be potential exploration targets if the lacustrine shales have suitable geologic conditions. Lacustrine shales are widely developed in China, such as Qingshankou Formation (Songliao Basin), Chang 7 member (Ordos Basin), Shahejie Formation (Bohai Bay Basin), and Lucaogou Formation (Junggar Basin) (Liang et al., 2017; Huang et al., 2020a; Hu et al., 2022b). At present, these key horizons have achieved breakthroughs in the shale oil field, especially in the enrichment mechanism, occurrence state, sweet spot selection, and evaluation (Liang et al., 2017; Zhang et al., 2019; Guo et al., 2021; Hu et al., 2021a; Jin et al., 2022; Wu et al., 2022a). Meanwhile, in the engineering field, horizontal well and volume fracturing, as

[1]China University of Petroleum, State Key Laboratory of Petroleum Resources and Prospecting, Beijing, China; China University of Petroleum, College of Geosciences, Beijing, China; and University of Calgary, Department of Chemical and Petroleum Engineering, Calgary, Canada. E-mail: wuyuping23@163.com.

[2]China University of Petroleum, State Key Laboratory of Petroleum Resources and Prospecting, Beijing, China and China University of Petroleum, College of Geosciences, Beijing, China. E-mail: liucl@cup.edu.cn (corresponding author); jiangfj@cup.edu.cn; thu@cup.edu.cn; 1140714719@qq.com; 18811135611@163.com; 15908314132@163.com; 18724415345@163.com; 541728149@qq.com.

[3]Hefei University of Technology, School of Resources and Environmental Engineering, Hefei, China. E-mail: rsageoche@gmail.com.

Manuscript received by the Editor 6 June 2022; revised manuscript received 4 October 2022; published ahead of production 24 November 2022; published online 27 January 2023. This paper appears in *Interpretation*, Vol. 11, No. 1 (February 2023); p. T145–T159, 15 FIGS., 2 TABLES.
http://dx.doi.org/10.1190/INT-2022-0060.1.

well as in-situ heating conversion in organic-rich shale, are constantly being tested (Hu et al., 2020). However, due to insufficient research on hydrocarbon generation (HG), hydrocarbon expulsion (HE), and hydrocarbon retention (HR) mechanism of lacustrine shales, the prediction of hydrocarbon-enriched sweet spots and shale oil resource potential has not been well explained.

The HG and HE processes are extremely complex (Chen et al., 2015; Huang et al., 2017; Xue et al., 2022). Previous studies have shown that there are principally two factors that control HG and HE: (1) organic matter (OM) properties, i.e., organic abundance, kerogen type, and thermal maturity, and (2) inorganic characteristics, i.e., mineral constituents, fractures, formation temperature, and pressure, etc. (Huang et al., 2017, 2020b, 2021; Milliken et al., 2021; Xue et al., 2022). Many researchers have tried to analyze the HG and HE processes of source rocks using different approaches. Physical simulation experiments, such as the gold tube simulated thermal experiment, can be used to evaluate the HG and HE (Xiang et al., 2016). However, due to the differences between the heating rate and experimental condition parameters, the calculated results may be quite different from the geologic conditions (Zheng et al., 2019; Xue et al., 2022). Some scholars also use basin modeling software (e.g., PetroMod) to study the HG and HE characteristics of source rocks (Hakimi et al., 2020). However, PetroMod requires many key parameters that rely on physical simulation experiments, such as kinetic parameters. Pang et al. (2005) propose a hydrocarbon generation potential (HGP) method based on the mass-balance approach. It can be used to quantitatively analyze the characteristics of HG and HE during geologic history. Moreover, the method requires only a few easily accessible parameters (abundant pyrolysis data). Thus, the HGP method has been widely used in many basins (Zheng et al., 2019; Chen et al., 2020). In this study, the HGP method was used to evaluate the HG and HE characteristics of the Fengcheng Formation (P_1f) in the Junggar Basin.

The Junggar Basin is located in northwest China and comprises abundant petroleum resources (Cao et al., 2006; Liu et al., 2016). The P_1f and Wuerhe Formation (P_2w) are the most important source rocks in the Mahu sag (Liu et al., 2016; Xiang et al., 2016; Tao et al., 2019; Wu et al., 2022a). Among them, the P_1f source rock is the most famous and is considered to be deposited in the oldest-known alkaline lake globally (Yu et al., 2019; Cao et al., 2020). Compared with traditional lacustrine sediments, the alkaline lacustrine environment can induce the development of a large number of special biological species, including bacteria and algae (Cao et al., 2020; Guo et al., 2021), resulting in the enrichment of OM and the formation of high-quality source rocks (Guo et al., 2021). In recent years, the PetroChina Xinjiang Oilfield continuously expanded oil and gas exploration areas, and drilling has been carried out in the deep sedimentary units of the Mahu sag. Active oil and gas displays and industrial oil production indicate that P_1f has considerable shale oil resources (Tang et al., 2021b). In addition, the core samples produced by these wells provide an opportunity to study the HG and HE mechanisms of the shales. Moreover, alkaline lake source rocks differ from traditional freshwater and saltwater lake source rocks, but it is unknown whether their HG models are consistent with traditional models. Therefore, the evaluation of HG and HE of the P_1f is a controversial subject that needs to be resolved and urgently needs to be studied. This research analyzes the HG and HE characteristics of the P_1f shale and evaluates the shale oil resource potential in combination with the known geologic conditions.

Geologic setting

The Junggar Basin is the second-largest sedimentary basin in northwestern China, covering an area of approximately 1.3×10^5 km^2 (Figure 1a) (Wu et al., 2014; Guo et al., 2021). The basin presents a triangular shape, surrounded by the Qinggridi Mountains to the east, the Zaire Mountains to the west, the Yilinheibiergen and Bogda Mountains to the south, and the Altai Mountains to the north (Figure 1b) (Tang et al., 2021a; Wu et al., 2022b). It is a large superimposed basin that has undergone many cycles of tectonic evolution during geologic history (Wu et al., 2014; Yu et al., 2019; Imin et al., 2020; Tang et al., 2021a). There are six different tectonic units in the basin (Figure 1a). The Mahu sag is located in the northwestern part of the central depression, with an exploration area of approximately 5000 km^2 (Figure 1b). It is adjacent to the fault zone in the northwest, the Zhongguai uplift in the southwest, and the Dabasong and Xiayan uplifts in the southeast (Wu et al., 2022b). At present, the sag appears to be a monoclinic slope in the southeast direction. There are multiple sets of source rocks developed in the Mahu sag (Figure 2). Among them, P_1f is the most important source rock, forming several large oil and gas fields (Cao et al., 2006; Tao et al., 2019; Tang et al., 2021b).

Samples and methods

Samples and experimental methods

In this study, 188 core samples are selected from diverse wells. Most of these rocks are formed in shallow lake areas and deeper lake facies. This study uses the total organic carbon (TOC) content, Rock-Eval pyrolysis, and organic petrology analysis to determine the OM abundance, kerogen type, and thermal maturity. All experiments were carried out at the State Key Laboratory of Petroleum Resources and Prospecting, China University of Petroleum (Beijing).

The samples are initially surface-cleaned and then ground to 200 meshes before TOC and pyrolysis experiments. A small amount of the powdered sample (0.10 g) is analyzed using a LECO CS230 apparatus that can investigate the TOC content. The process of pyrolysis is as follows: the sample is divided into two fractions after being crushed to powder. The first fraction is directly used for the pyrolysis experiment. The second fraction is used for pyrolysis after approximately seven days of

solvent extraction with dichloromethane. The pyrolysis experiment is carried out using a Rock-Eval VI instrument. Initially, the temperature of pyrolysis was maintained at 300°C, and then the pyrolysis temperature was raised to 600°C at an interval of 25°C/min. The free hydrocarbon S_1, the cracking hydrocarbon of kerogen S_2, and the thermal maturity parameter T_{max} are obtained.

The vitrinite reflectance (Ro) and maceral composition examinations were carried out under a microscope equipped with fluorescence illuminators. The polished blocks were performed under oil immersion and irradiated with monochromatic light. According to literature standards, Ro < 0.5%, 1.0% < Ro < 1.2%, and Ro > 1.2% represent the immature, mature, and postmature stages, respectively (Hakimi and Ahmed, 2016).

Method of TOC recovery

The OM abundance of source rocks can be changed during the process of HG (Jarvie et al., 2007). When the residual total organic carbon (TOC_R) is used to evaluate the quality of source rocks, errors will inevitably be caused. Thus, restoring the TOC_R to the original TOC (TOC_O) is necessary. The TOC_O can be used to quantitatively evaluate key parameters such as the HGP and the OM porosity (Jarvie et al., 2007; Chen et al., 2015). The TOC_R at different stages of maturity is used in the following equation (Romero-Sarmiento et al., 2013):

$$TOC_O = TOC_R + TOC_E, \quad (1)$$

where TOC_E is the quantity of organic carbon contained in the expelled hydrocarbons (%).

HG is a process in which organic carbon is thermally degraded and converted into hydrocarbons. As the maturity increases, part of the TOC_O will be converted into hydrocarbons and expelled from the source rock. Consequently, the TOC_R will gradually decrease (Chen et al., 2015). However, there are two parts of TOC_O in the source rock (Figure 3): (1) reactive carbon (TOC_{rea}) can generate hydrocarbons under thermal maturation and (2) nonconvertible carbon (TOC_{Ine}) cannot be converted into hydrocarbons (Jarvie et al., 2007). In general, nonconvertible carbon cannot be thermally degraded (Romero-Sarmiento et al., 2013). Meanwhile, due to the different HGP of various types of kerogen, their conversion efficiency to hydrocarbons is diverse. This feature in the HG process of source rocks can be reflected by the degradation rate of kerogen (D), where $D = TOC_{rea}/TOC_O$, the ratio of reactive carbon to initial organic carbon.

The residual HGP of the source rock is transformed from $TOC_{R\text{-}rea}$, which is related to the remaining degradation rate of kerogen (D_R) (Chen et al., 2015). Thus, the following equations are obtained

$$D_R = TOC_{R\text{-}rea}/TOC_R, \quad (2)$$

$$TOC_{R\text{-}rea} = 0.083 \times (S_1 + S_2). \quad (3)$$

After transformation,

$$D_R = 0.083 \times (S_1 + S_2)/TOC_R, \quad (4)$$

where $TOC_{R\text{-}rea}$ represents the remaining convertible organic carbon, with 0.083 as the average carbon in hydrocarbons.

During the HG process, it is assumed that the absolute content of inert carbon remains unchanged (Romero-Sarmiento et al., 2013). Moreover, the following relationships can be obtained

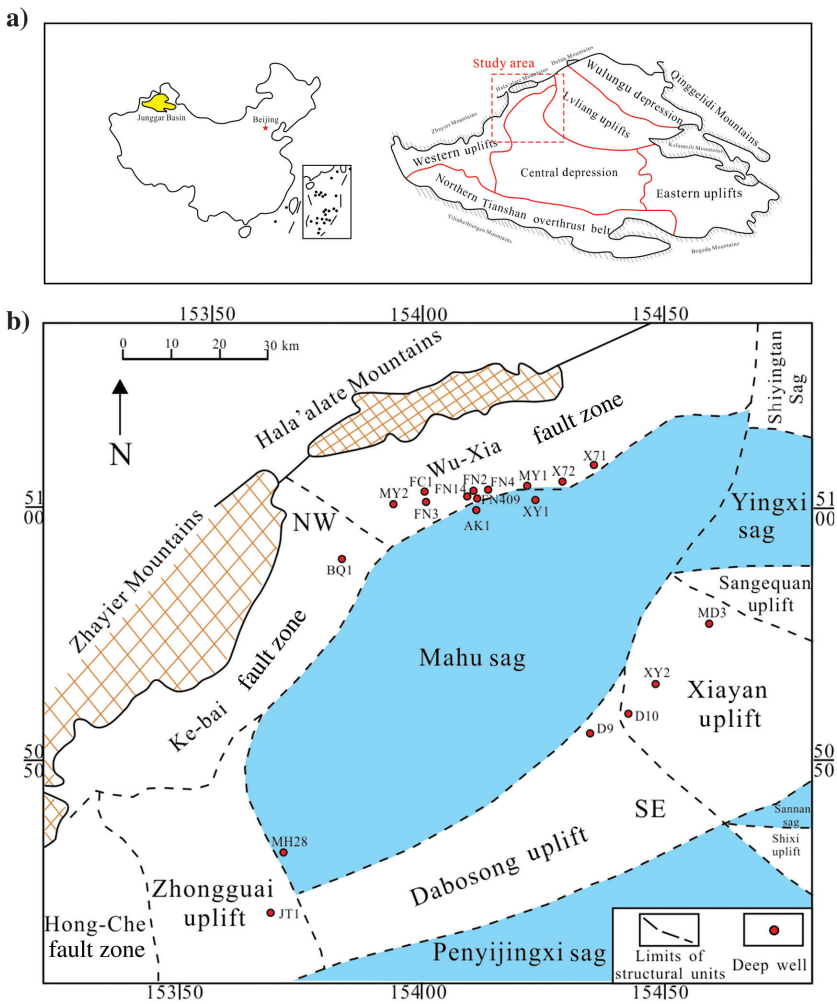

Figure 1. (a) The location and structural units of the Junggar Basin and (b) the location of structural units and wells in the sag (after Tao et al., 2019).

$$\mathrm{TOC}_o(1-D_o)=\mathrm{TOC}_r(1-D_r), \tag{5}$$

$$(1-D_r)/(1-D_o)=\mathrm{TOC}_o/\mathrm{TOC}_r. \tag{6}$$

The recovery coefficient k of TOC can be expressed as

$$k=\mathrm{TOC}_o/\mathrm{TOC}_r. \tag{7}$$

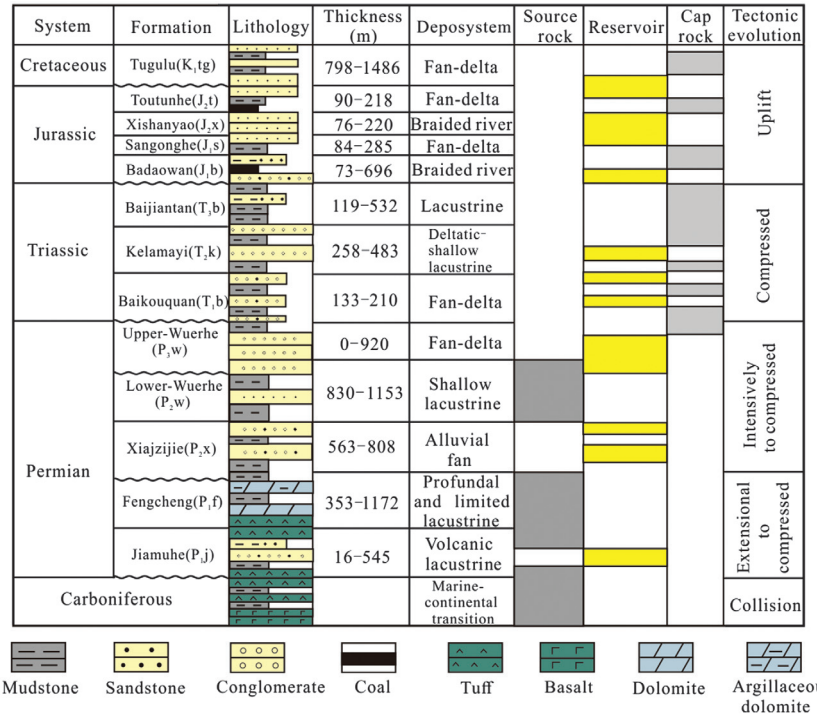

Figure 2. The stratigraphic column in the Mahu sag (modified after Feng et al., 2020).

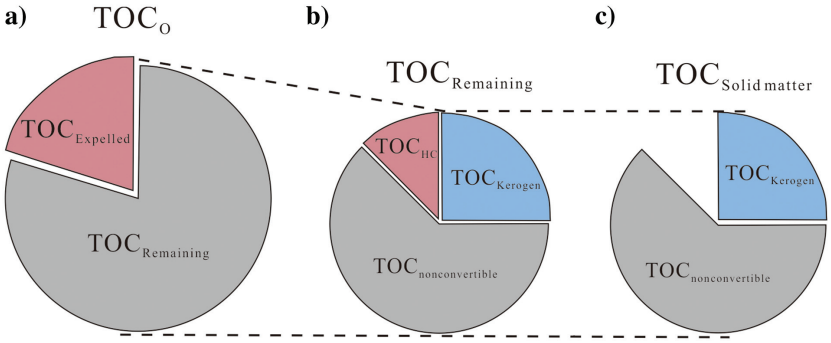

Figure 3. Model of TOC during thermal maturation (modified after Romero-Sarmiento et al., 2013). (a) TOCo is composed of organic carbon that has been converted into hydrocarbons and carbon remaining in the rock, (b) the distribution characteristics of reactive carbon ($\mathrm{TOC_{R\text{-}rea}}$ = $\mathrm{TOC_{HC}}$ + $\mathrm{TOC_{Kerogen}}$) and nonconvertible carbon ($\mathrm{TOC_{Ine}}$) in source rocks undergo HE, and (c) the $\mathrm{TOC_{Rem}}$, including $\mathrm{TOC_{Ine}}$ and $\mathrm{TOC_{R\text{-}rea}}$ (which also can be expressed as $\mathrm{TOC_{Kerogen}}$).

The original degradation rate (D_O) is related to the type of kerogen. The D_O of each type of kerogen is approximately equal to the D_R distribution's top limit for that type of kerogen (Chen et al., 2015). The kerogen type in the P_1f shale is determined by the crossplot between T_{max} and hydrogen index (HI) (Figure 4a). The D and T_{max} of various kerogen types are shown in Figure 4b. Moreover, this research established the distribution characteristics of D_O and D_{Rem} of various types of kerogen when they enter the hydrocarbon generation threshold (HGT). According to the examined sample data set, the D_O values of type I, II_1, II_2, and III kerogens are 0.90, 0.70, 0.60, and 0.30, respectively. The TOC recovery coefficient k can be calculated according to equation 5.

HG and HE model

In this study, the HGP model proposed by Pang et al. (2005) is used to quantitatively analyze the P_1f shale (Figure 5). It is believed that the HGP of source rocks remains unchanged until the generated hydrocarbons are expelled during the maturation process. When hydrocarbons begin expelling from the source rocks, the HGP will gradually decrease (Pang et al., 2005; Chen et al., 2020). Therefore, the HE process can be investigated by analyzing the change in HGP.

In general, the HGP can be expressed by obtaining the pyrolysis parameters (S_1 + S_2). The HGP index (P_g) is expressed as (S_1+S_2)/TOC, which indicates the number of hydrocarbons generated per unit of organic carbon. It includes the amount of retained hydrocarbons within shales and the hydrocarbons that can be converted as maturity increases (Pang et al., 2005). The P_g is called the original HGP index (P_{go}) when the source rock does not expel hydrocarbons. However, when the expulsion of hydrocarbons begins, the P_g gradually decreases, and then it is called the residual HGP index (P_{gr}).

Thus, the change of P_g can be used to calculate the HE ratio (P_e), the HE rate (V_e), and HE efficiency (R_{ef}). The equations are as follows:

$$P_e(R_o)=P_{go}(R_o)-P_{gr}(R_o), \tag{8}$$

$$V_e(R_o)=\Delta P_e/\Delta R_o, \tag{9}$$

$$R_{ef}(R_o)=100\times P_e(R_o)/P_{go}(R_o). \tag{10}$$

Based on this analysis, the HG and HE intensity of source rocks can be calculated by equations 11 and 12:

$$E_g = \int_{R_{o1}}^{R_o} 10^{-3} \times P_{go}(R_o) \times H \times \rho \times \mathrm{TOC}_o(R_o) dR_o, \quad (11)$$

$$E_e = \int_{R_{o2}}^{R_o} 10^{-3} \times P_e(R_o) \times H \times \rho \times \mathrm{TOC}_o(R_o) dR_o, \quad (12)$$

where E_g and E_e are the intensity of HG and HE ($\times 10^4$ t/km^2), respectively; R_{o1} is the HGT (%); R_{o2} is the HET (%); H is the thickness of the shale (m); ρ is the density of the shale (g/cm^3), and A is the area of the shale (m^2).

Monte Carlo method

The Monte Carlo method, known as the statistical simulation method, is used to simulate a probability statistical model of a given problem by random sampling and gives the statistical estimate of the numerical solution of the problem (Cortazar and Schwartz, 1998; Yang et al., 2008). The evaluation of mineral resources possesses a random feature due to the nature of random variables in geologic observation results, and any result should have a certain probability sense. Therefore, the probability distribution of the parameters of resource assessment can be studied using statistical skills, and the probability value of the parameters can be assigned. In general, these parameters can be represented mathematically by models such as uniform, triangular, normal distribution, etc. The Monte Carlo method can simulate random variable distributions. By using this method, the probability distribution of resources can be improved. Moreover, this method can overcome the uncertainty of resource evaluation parameters and ensure the scientific rationality of evaluation results. A detailed Monte Carlo simulation process can be found in Yang et al. (2008).

Result and discussion

Geologic and geochemical characteristics of the source rocks

Lithology and thickness

During the Permian period, fine-grained lacustrine deposits are well developed in the Mahu sag. It comprises complex and varied lithologic combinations: (1) marginal shallow lake facies argillaceous sandstone, (2) semideep lacustrine facies, (3) deep lacustrine facies shale, (4) argillaceous limestone, and (5) argillaceous dolomite (Figure 6). Predecessors predicted the distribution of P_1f shale in the Mahu sag based on drilling data, sedimentary facies, and seismic interpretation (Tao et al., 2019). As is shown in Figure 6, the P_1f shale is distributed throughout the sag, with a thickness of 50–300 m, averaging more than 100 m. However, the thickness of the P_1f shale is quite different between the deposition center and the periphery. The thickness shows a thinning trend from the northwest to the south-

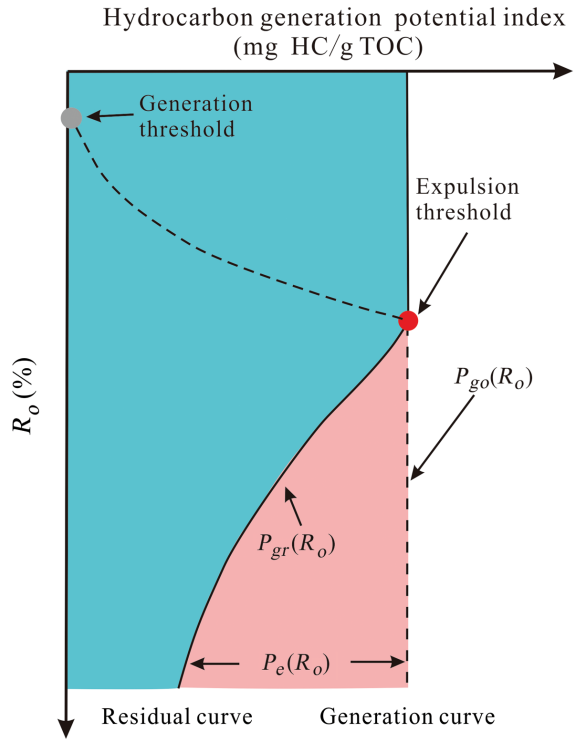

Figure 5. Model of the source-rock HG and HE (modified after Pang et al., 2005).

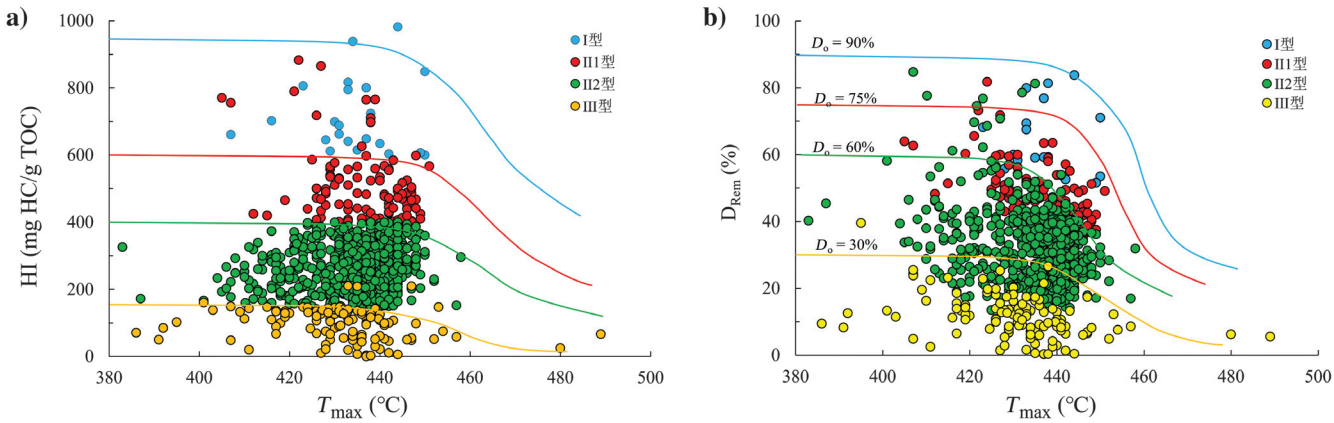

Figure 4. The crossplots of HI and the D_{Rem} with T_{max} for different kerogen types from the P_1f shale. Note: part of the data is from the PetroChina Xinjiang Oilfield Company.

east and reaches the maximum in the fault zone, which is consistent with the nature of its special foreland basin (Tao et al., 2019; Yu et al., 2019; Imin et al., 2020). Despite the poor wells in the depocenter, the thickness of the shale in the sag's depocenter is believed to be larger than 300 m based on a peripheral investigation. These organic-rich shales provide favorable conditions for hydrocarbons formation.

OM abundance

The OM abundance is one of the key parameters for evaluating the potential of the source rock. It can be evaluated by TOC, petroleum yield (S_1 + S_2), and chloroform bitumen "A" (Hakimi and Ahmed, 2016). In general, the higher the TOC and petroleum yield, the higher the HGP (Xue et al., 2022). The TOC of the P_1f shale mainly varies from 0.4 wt% to 4.0 wt%, averaging 0.80 wt% (Figure 7a). The overall distribution of petroleum yield is between 2.0 and 8.0 mg HC/g rock, averaging 3.95 mg HC/g rock (Figure 7a). The chloroform bitumen A ranges from 0.01% to 0.19%, averaging 0.24% (Figure 7b). These parameters indicate that the P_1f has good HGP.

The contour map of the original TOC was obtained using the following process. The measured TOC data are rich in the northern area. The percentage of various kerogen types in a single well was first determined, and the recovery coefficient was then calculated according

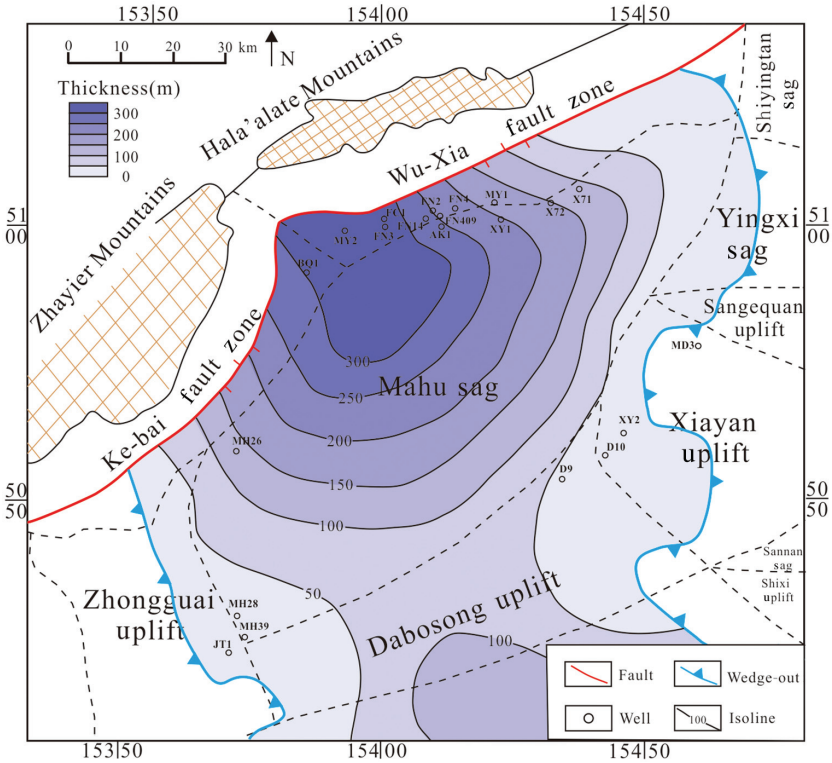

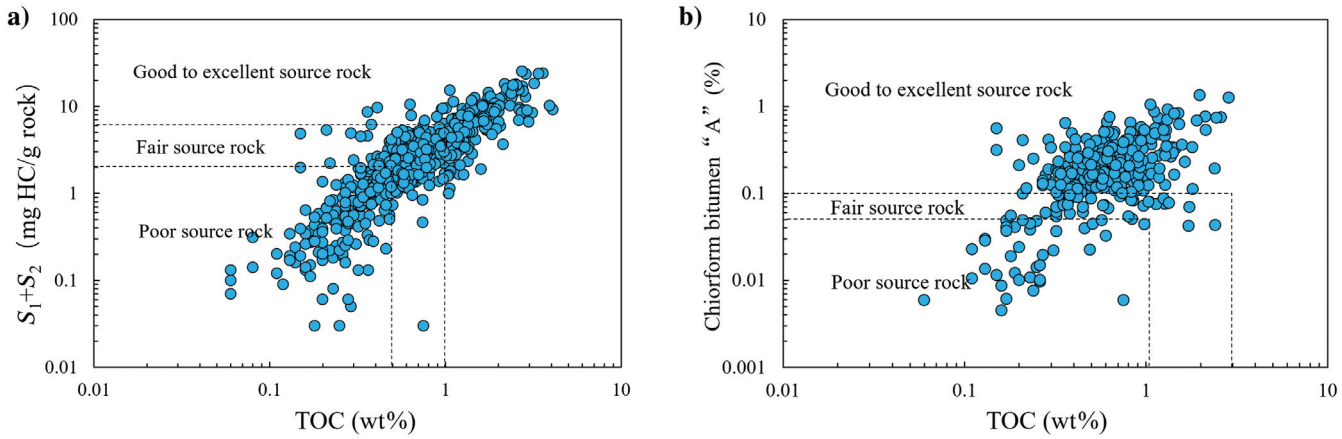

Figure 6. Thickness distribution of P_1f source rocks in the Mahu sag.

Figure 7. Geochemical characteristics of the P_1f shale. (a) Crossplot of TOC versus (S_1 + S_2) and (b) crossplot of TOC versus chloroform bitumen A.

to equation 7. As a result, the original TOC of a single well was calculated according to the weighting factor of kerogen. However, the rest of the sag can only be extrapolated by sedimentary characteristics due to the lack of drilling wells. Figure 8 shows the TOC_O distribution of P_1f shale. The higher TOC_O is mainly distributed in the northwest, corresponding to the depocenter. The maximum TOC_O of this set of source rocks can exceed 4.0 wt%.

Kerogen type

The identification of kerogen type is important for evaluating a source rock because it affects the composition and scale of HG during the maturity process

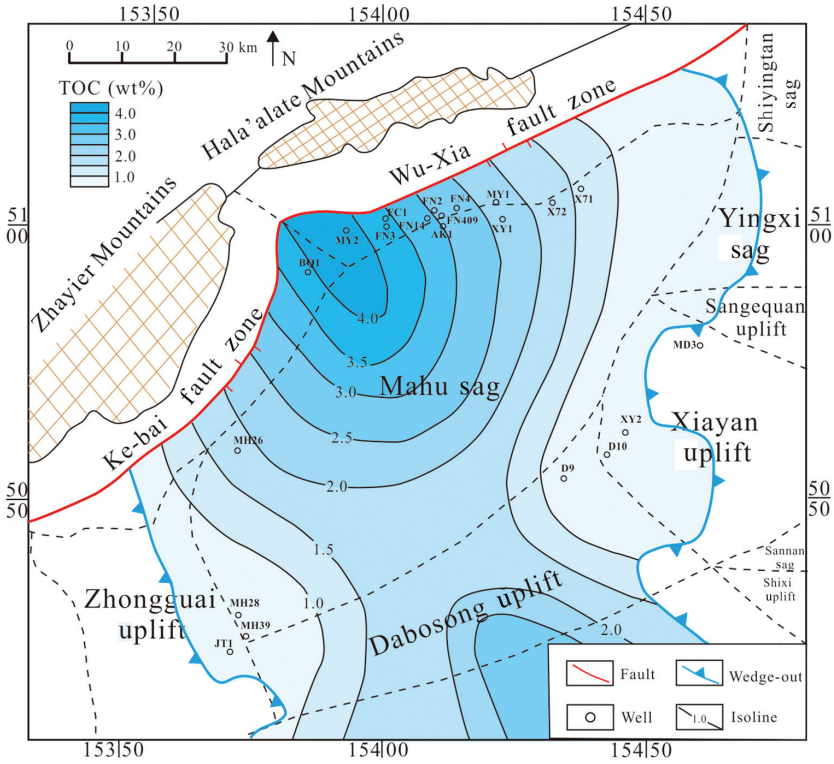

Figure 8. Original TOC distributions of the P_1f shale.

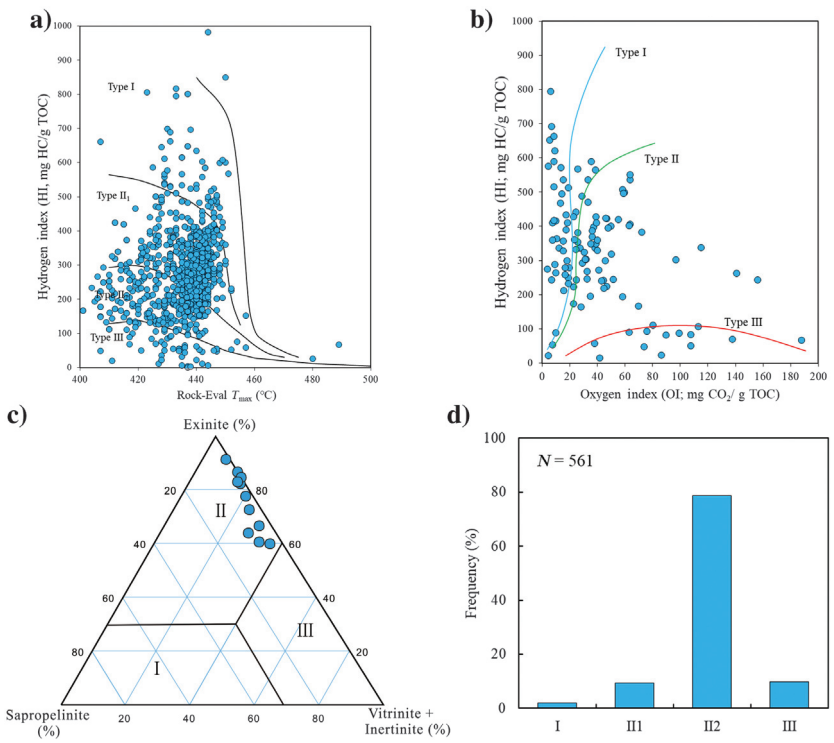

Figure 9. Diagrams showing the kerogen types. (a) HI versus T_{max} (after Hakimi and Ahmed, 2016), (b) HI versus OI (after Hakimi and Ahmed, 2016), (c) the ternary diagram of maceral composition (after Wang et al., 2015), and (d) frequency diagrams of kerogen type of well MY1.

(Wu et al., 2014; Hakimi and Ahmed, 2016). The type of kerogen in the examined shale is evaluated using the extensive evaluation procedures in this study.

The van Krevelen diagram (HI versus oxygen index [OI]) and the crossplot of HI versus T_{max} are used to classify the kerogen type (Hakimi and Ahmed, 2016).

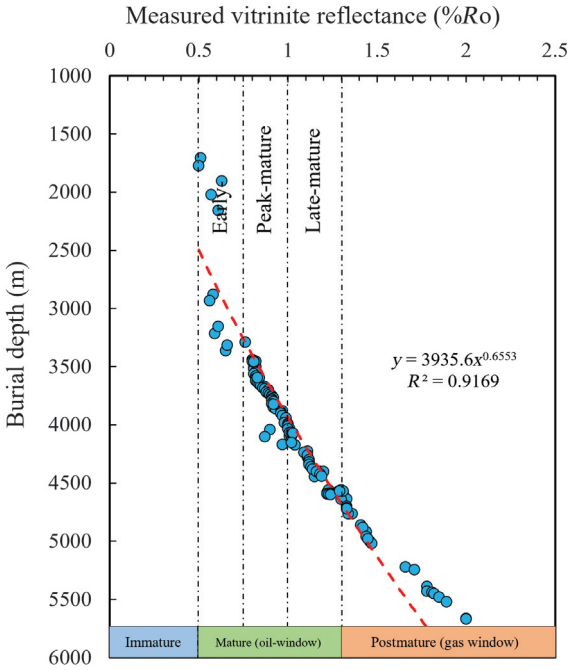

Figure 10. Diagram of the thermal evolution degree of the P_1f.

The crossplot between HI and T_{max} shows that the shale is dominated by type II kerogen (Figure 9a), consistent with the HI versus OI plot (Figure 9b). Kerogen type also can be determined using organic maceral components (Wang et al., 2015; Hakimi and Ahmed, 2016; Hakimi et al., 2020). The results of microscopic identification revealed that the P_1f shale mainly contains exinite and vitrinite (Figure 9c). However, the exinite maceral group is significantly higher. It shows that the OM mainly comes from higher plants and algae. These results are consistent with the geochemical data, indicating that this set of mudstone mainly contains type II kerogen (Figure 9d), which tends to generate oil during maturation.

Thermal maturity

Thermal maturity is another essential metric for evaluating the potential of source rocks (Wu et al., 2014). The Ro and T_{max} are widely used as maturity indicators (Hackley et al., 2015; Hakimi and Ahmed, 2016; Katz and Lin, 2021). Compared with T_{max}, R_o is more reliable to characterize the maturity of source rocks (Hackley et al., 2015; Katz and Lin, 2021).

The plot of R_o versus burial depth of the examined samples shows an increasing trend of R_o as the depth increases (Figure 10). The R_o reaches 0.5% at approximately 1800 m, which means that the P_1f shale has entered the mature stage. The depth of P_1f in the study area is relatively shallow (<5000 m), which does not reflect the full range of source rock maturity. Thus, the established relationship between measured R_o and burial depth (h) can be presented as $Ro = 2.0 \times 10^{-5} h^{1.3057}$, where

Figure 11. Ro distributions of the P_1f shale.

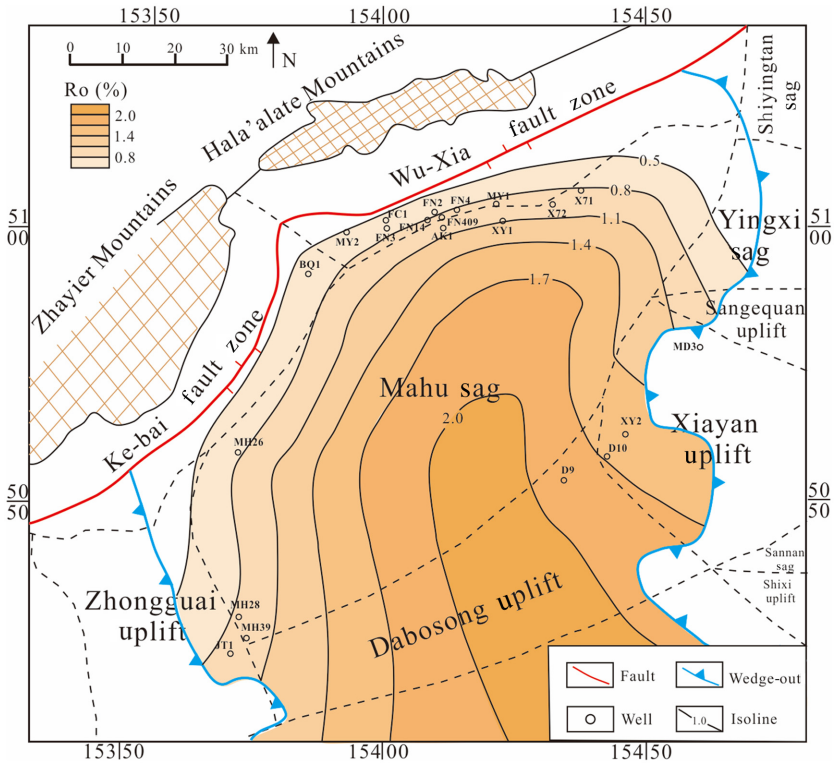

R^2 = 0.9169. This mathematical relationship is based on the measured data of 141 core samples from 18 wells. Using the structural contour map of the P_1f shale, a contour map of the R_o of the source rock is shown in Figure 11. Overall, the R_o is greater than 1.1% in most of the area, with the maximum R_o > 1.8% in the sag's central area.

HG and HE characteristics

HG and HE model of P_1f *source rocks*

An HG and HE model of P_1f shale are established based on the collected data. Primarily, the envelope curve of the $P_{gr}(R_o)$ and $P_{go}(R_o)$ is obtained using the $(S_1 + S_2)$/TOC data (Figure 12a). Then, the key parameters such as the expulsion ratio, expulsion rate, and expulsion efficiency can be obtained through equations 8–10.

In general, 0.5%Ro is considered the threshold for HG. Pang et al. (2005) propose the expulsion threshold Ro when hydrocarbons began to be expelled. According to the established geologic model, the hydrocarbon expulsion threshold (HET) of the P_1f shale is approximately 0.80%Ro, with a depth of approximately 3500 m (Figure 12a). The source rock begins to expel a large number of hydrocarbons once the HET is reached. The P_e rose rapidly in the early stage and tended to be flat in the subsequent stage (Figure 12b). The V_e initially showed a rapid rise and then a declining trend, reaching a peak at 1.40%Ro (Figure 12c). As the thermal maturity increases, the R_{ef} of the P_1f shale also gradually increases. When the Ro of the shale increases from 0.80% to 1.60%, the R_{ef} increases from 0% to 66% (Figure 12d). Similar to the P_e trend, the R_{ef} trend rapidly rises initially and then slowly increases.

HG and HE intensity of P_1f *source rocks*

The HG and HE intensity of source rocks are calculated by the method explained in the "Samples and methods" section. Figure 13 shows that the P_1f shale has reached the HGT. Moreover, the entire sag has a potential for HG and the intensity of HG varies in different areas. The center of the HG intensity is on the northwestern edge of the sag with a maximum value of 1200 × 10^4 t/km^2 (Figure 13a). The intensity of HG in the eastern part of the sag is relatively low, generally less than 400 × 10^4 t/km^2 (Figure 13a). Similarly, the HE characteristics of the P_1f shale also are evaluated (Figure 13b). The HE range of this set of the source rock is relatively higher due to the relatively higher burial depth and a high degree of evolution. The HE center is located in the southern area of well AK1, and the maximum HE intensity is 600 × 10^4 t/km^2 (Figure 13b). It indicates that a large number of hydrocarbons are still retained in the P_1f shale and have not yet been expelled. In other words, the P_1f shale has enormous shale oil and gas potential.

The HG and HE history of the P_1f have been restored by combining the study area's burial and thermal evolution history. The formation thickness, sedimentary age, and denudation data are collected based on drilling reports. The heat flow data in the Mahu sag are collected from previous works (Xiang et al., 2016). It can be seen that the Ro of the source rock reached 0.50% in the late Permian due to the rapid burial and the high heat flow (Figure 14). In the Early Triassic, the Ro reached 0.70% and massive hydrocarbons began to be generated from the mature source rock. The thermal maturity was higher (Ro > 0.80%) in the Late Triassic, and a large amount of mature petroleum was formed and expelled from the source rock. The maturity of source rocks has gradually increased since the Triassic, whereas the rate of HG has significantly decreased. At present day, thermal maturity has entered a mature to the high-mature stage.

Shale oil resource assessment

Usually, the volumetric method is used to directly evaluate shale oil resources, which is more convenient than other methods. Shale is a complex aggregate of OM and inorganic minerals. The physical states of hydrocarbons in shale are very complex, including various

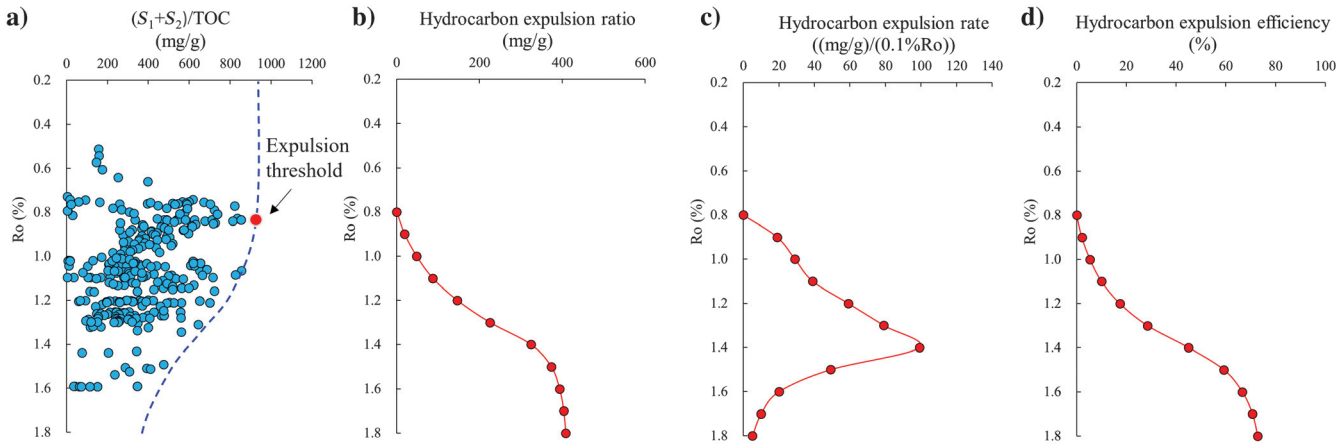

Figure 12. The HG and HE model of the P_1f shale: (a) $(S_1 + S_2)$/TOC versus Ro profile, (b) changes in HE ratio, (c) changes in HE rates, and (d) changes in HE efficiency.

phases (Zhang et al., 2019; Hu et al., 2021b). Among them, the free and adsorbed phases are considered to be the most important states. The free oil resources are theoretically the largest recoverable resources. Therefore, several analytical methods on the adsorption behavior of hydrocarbons within shales have been recently proposed (Jarvie, 2012; Li et al., 2019; Huang et al., 2020a). However, when estimating the adsorption capacity of shale oil, determining the adsorption coefficient becomes very important. Previous studies have confirmed that OM has an important influence on the adsorption capacity of hydrocarbons. In general, 100 mg HC/g TOC is the upper limit of saturated hydrocarbon adsorption (Jarvie, 2012). However, it might not be appropriate to use this critical value in lacustrine shale. The predecessors proposed to use the two-step pyrolysis method to characterize the total oil yield and the adsorbed oil yield within shales (Jarvie, 2012; Abrams et al., 2017). The method was used to evaluate the total oil and free oil of the P_1f shale:

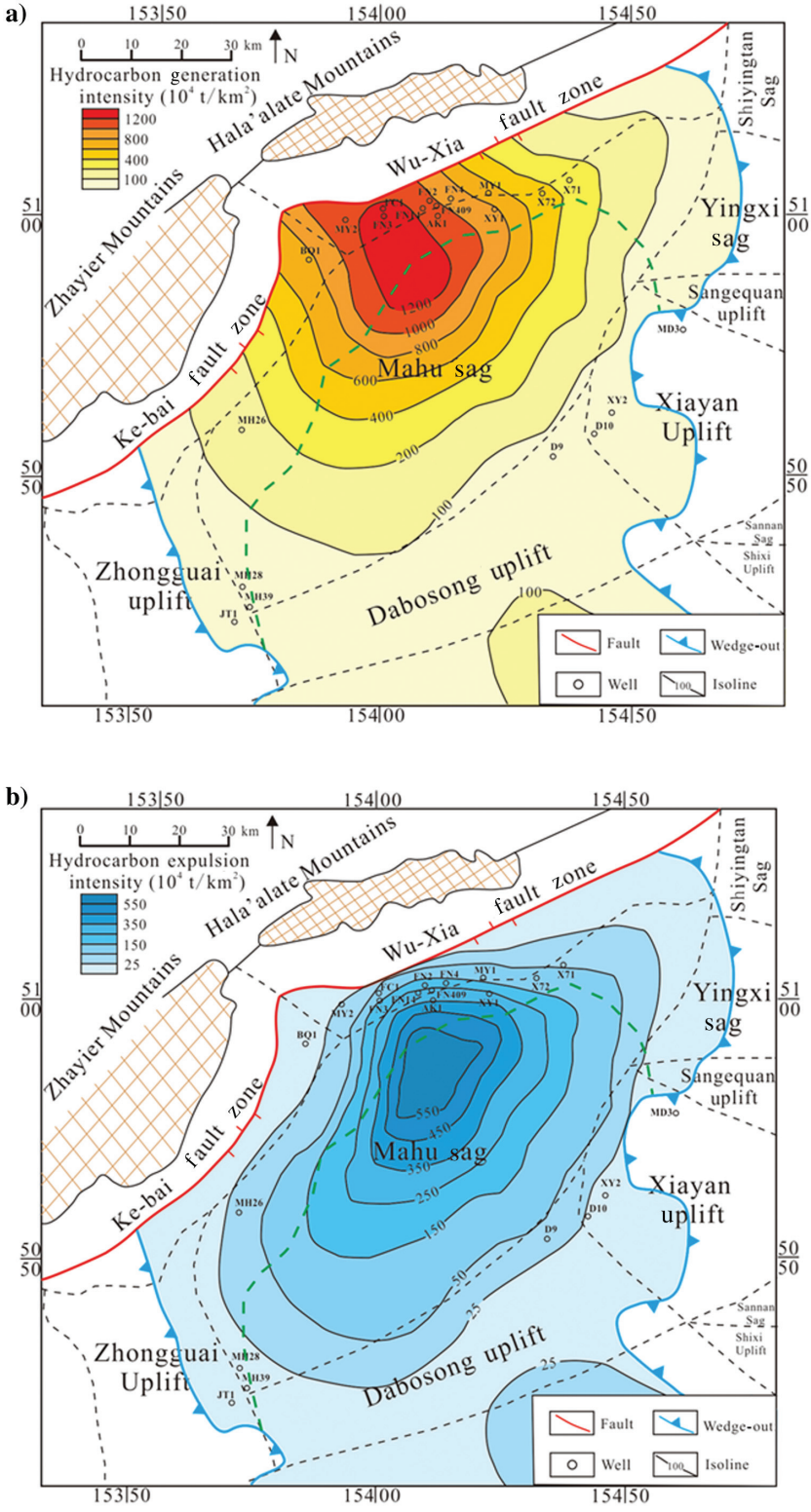

Figure 13. Contour maps showing (a) HG intensity and (b) HE intensity of P_1f shale. The dotted green line represents the contour lines of 5500 m.

$$\text{Total oil yield} = (S_1 - S_{1\text{extracted}}) + (S_2 - S_{2\text{extracted}}) + S_{1\text{Loss}}, \quad (13)$$

$$\text{Free oil yield} = S_1 + S_{1\text{Loss}}. \quad (14)$$

In these equations, $S_{1\text{Loss}}$ is the loss of light hydrocarbons ($<C_{15-}$). Previous studies have shown that the loss of light hydrocarbons is related to the API gravity of oil, where API gravity = $0.412 \times C_{15-}$ (wt%) + 20.799 (Michael et al., 2013). The density of petroleum produced in the P_1f shale is collected by Tang et al. (2021b). Thus, the light hydrocarbon recovery coefficient is calculated using the proposed equation, which is approximately 28% of S_1.

According to the experimental results (Table 1), the total oil content is approximately 3.42 mg/g, with free oil accounting for 60% of the total oil at 2.06 mg/g. It is suggested that the burial depth of shale in the favorable area should be less than 5500 m, and the favorable area is approximately 3000 km^2. After determining the key parameters, the volumetric method is used to calculate the resources:

$$Q_{\text{TOY}} = S \times h \times \rho \times S_{1\text{correction}}, \quad (15)$$

where Q_{TOY} is the total resource of shale oil (10^4 t), S is the effective area of shale (km^2), h is the thickness of shale (m), and ρ is the shale density (2.60 t/m^3).

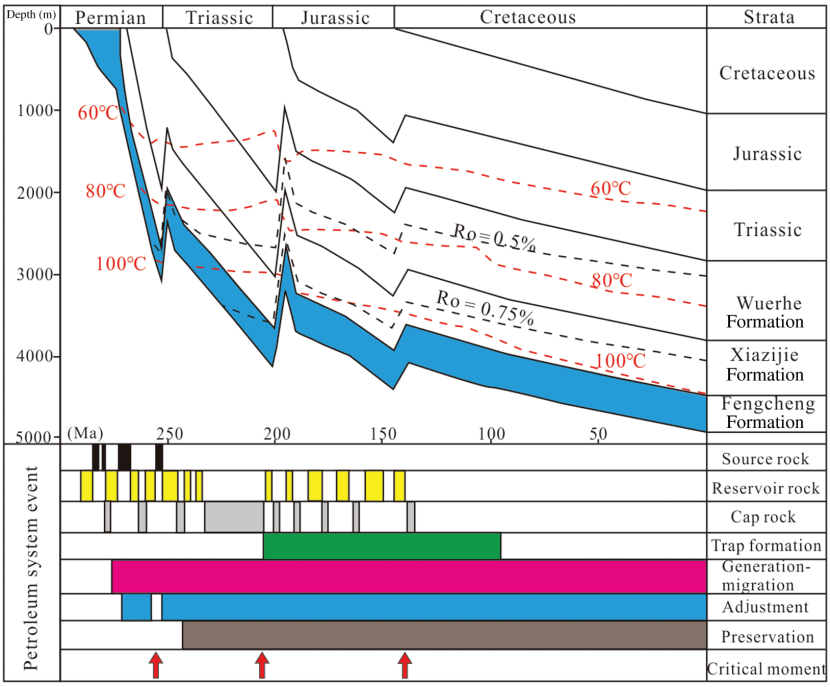

Figure 14. Burial and thermal evolution histories of well MY1 (modified after Cao et al., 2006; Wu et al., 2022b).

Table 1. Rock-Eval data set for whole rock and the solvent extracted samples.

Sample ID	TOC (wt%)	Whole rock sample			Postsolvent extracted sample			S_{1Loss} (mg/ g)	Total oil (mg/g)	Free oil (mg/g)
		S_1 (mg/g)	S_2 (mg/g)	T_{max} (°C)	S_1 (mg/g)	S_2 (mg/g)	T_{max} (°C)			
1	2.328	4.03	9.01	435	0.10	4.00	443	1.13	10.07	5.16
2	0.587	0.86	1.52	438	0.07	0.71	441	0.24	1.84	1.10
3	1.356	8.39	5.40	421	0.02	0.25	442	2.35	15.87	10.74
4	1.004	6.91	3.65	414	0.02	0.41	441	1.93	12.06	8.84
5	0.937	0.60	2.48	436	0.05	1.95	440	0.17	1.25	0.77
6	1.432	1.15	3.72	436	0.03	2.77	442	0.32	2.39	1.47
7	0.766	3.21	3.03	421	0.02	0.53	437	0.90	6.59	4.11
8	1.130	1.98	3.28	428	0.04	1.67	437	0.55	4.10	2.53
9	1.930	0.57	12.43	445	0.04	12.31	447	0.16	0.81	0.73
10	0.848	0.97	2.33	436	0.04	1.17	444	0.27	2.36	1.24
11	0.859	0.57	2.16	435	0.04	1.24	442	0.16	1.61	0.73
12	0.919	0.99	1.69	438	0.05	0.94	439	0.28	1.97	1.27
13	0.654	1.09	2.15	421	0.03	0.48	426	0.31	3.04	1.40
14	2.309	0.39	14.69	439	0.07	14.28	442	0.11	0.84	0.50
15	0.813	0.83	3.07	432	0.06	2.02	440	0.23	2.05	1.06
16	0.311	0.53	0.56	418	0.05	0.26	426	0.15	0.93	0.68
17	2.003	1.70	3.89	432	0.03	1.17	436	0.48	4.87	2.18
18	1.019	2.48	2.55	410	0.03	0.41	430	0.69	5.28	3.17
19	2.953	0.91	19.9	441	0.05	18.86	444	0.25	2.15	1.16
20	0.135	0.35	0.24	368	0.06	0.14	372	0.10	0.49	0.45
21	2.287	1.29	4.00	434	0.04	1.15	441	0.36	4.46	1.65
22	1.829	0.98	4.20	437	0.05	1.43	437	0.27	3.97	1.25
23	2.055	1.28	10.58	439	0.05	9.84	442	0.36	2.33	1.64
24	0.275	0.43	0.41	430	0.04	0.25	435	0.12	0.67	0.55
25	0.407	0.74	0.47	351	0.05	0.15	429	0.21	1.22	0.95
26	0.409	0.73	0.47	399	0.02	0.24	422	0.20	1.14	0.93
27	0.413	0.67	0.52	401	0.04	0.31	479	0.19	1.03	0.86
28	0.382	0.35	0.20	403	0.03	0.19	401	0.10	0.43	0.45

There are differences in the thickness of shale, TOC, and S_1 value in different regions. Monte Carlo is a method of uncertainty analysis, and it is an ideal method for solving the problem of parameter uncertainty (Cortazar and Schwartz, 1998; Yang et al., 2008). This method is widely used in resource estimation. Liu et al. (2014) use this approach to evaluate the shale oil resources in the northern Songliao Basin. Chen et al. (2020) use this method to estimate the probabilistic distributions of hydrocarbon resources in Jimusaer sag. This current study similarly used the Monte Carlo method to analyze the probability distribution of shale oil resources in the study area. After 2×10^8 random simulations, the probability distribution of shale oil resources of the P_1f shale was obtained (Figure 15; Table 2). The total shale oil geologic resources in the Mahu sag ranged from 6.52×10^8 t (with a probability of 90%) to 47.21×10^8 t (with a probability of 10%), averaging 23.30×10^8 t. The corresponding movable shale oil resources range from 3.85×10^8 t (with a probability of 90%) to 27.85×10^8 t (with a probability of 10%), with an average value of 13.75×10^8 t.

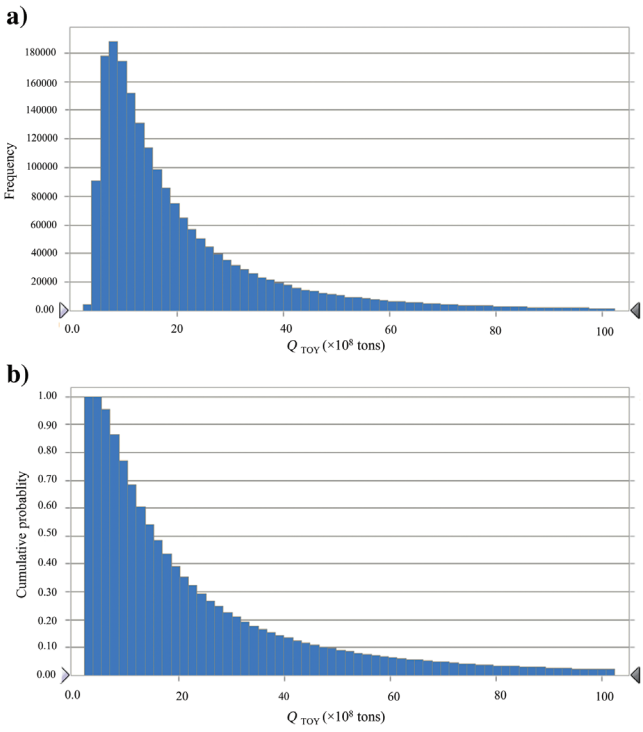

Figure 15. Statistical distributions of the estimated shale oil resource, showing the uncertainty of the estimate based on 2 million Monte Carlo simulations. (a) Frequency and (b) cumulative probability.

Conclusion

The Permian P_1f shale is a potentially valuable source rock. It has moderate TOC (average 0.80 wt%) and high petroleum yield (average 3.95 mg HC/g TOC), indicating fair to very good source-rock potential. Maturity data (Ro) suggest that the P_1f shale samples are mature to high-mature source rocks.

The HET of Fengcheng shale in Mahu sag is 0.80% Ro, and the peak of HE is 1.4%Ro. The maximum HG intensity is approximately 1200×10^4 t/km^2, and the maximum expulsion intensity is approximately 600×10^4 t/km^2. It indicates that a larger part of the retained hydrocarbons in the Fengcheng shale has not yet been expelled.

This research calculated the total oil yield of the shale and evaporative hydrocarbon loss to be 28% of the S_1. According to the Monte Carlo method, the total geologic resources (average) of shale oil are 23.30×10^8 t. The free oil resources (average) are 13.75×10^8 t, accounting for 60% of the total shale oil. Moreover, it reveals that the shale oil of the Fengcheng shale has good exploitation potential.

Acknowledgments

Financial support came from the Strategic Cooperation Technology Projects of CNPC and CUPB (ZLZX2020-01-05), the National Natural Science Foundations of China (41872127 and 41872128), the Science Foundation of China University of Petroleum (Beijing) (2462019BJRC005), the Young Talents Support Project of Beijing Science and Technology Association (ZX20210075), and the China Scholarship Council (CSC). We thank the PetroChina Xinjiang Oilfield Company for their assistance in providing the information in this study.

Data and materials availability

No data have been required for this paper.

Nomenclatures and abbreviations

HGP	=	Hydrocarbon generation potential
HG	=	Hydrocarbon generation
HE	=	Hydrocarbon expulsion
HR	=	Hydrocarbon retention
HGT	=	Hydrocarbon generation threshold, Ro (%)
HET	=	Hydrocarbon expulsion threshold, Ro (%)
TOC_R	=	Residual total organic carbon, wt%
TOC_O	=	Original total organic carbon, wt%

Table 2. Total and free oil resource estimates distributions of the P_1f shale.

	Probability distribution (%)									
Resource	90	80	70	60	50	40	30	20	10	Mean
Total oil ($\times 10^8$ t)	6.52	8.25	10.09	12.23	14.88	18.32	23.18	30.99	47.21	23.30
Free oil ($\times 10^8$ t)	3.85	4.87	5.96	7.22	8.78	10.81	13.68	18.29	27.85	13.75

TOC_E	=	The quantity of organic carbon contained in the expelled hydrocarbons, wt%
TOC_{rea}	=	Reactive carbon, wt%
TOC_{Ine}	=	Nonconvertible carbon, wt%
$TOC_{R\text{-}rea}$	=	Remaining convertible organic carbon, wt%
k	=	Recovery coefficient of TOC
D	=	Degradation rate of kerogen, %
D_O	=	Original degradation rate of kerogen, %
D_R	=	Remaining degradation rate of kerogen, %
P_g	=	HGP index, mg HC/g TOC
P_{go}	=	Original HGP index, mg HC/g TOC
P_{gr}	=	Residual HGP index, mg HC/g TOC

References

Abrams, M. A., C. Gong, C. Garnier, and M. A. Sephton, 2017, A new thermal extraction protocol to evaluate liquid rich unconventional oil in place and in-situ fluid chemistry: Marine and Petroleum Geology, **88**, 659–675, doi: 10.1016/j.marpetgeo.2017.09.014.

Cao, J., L. Xia, T. Wang, D. Zhi, Y. Tang, and W. Li, 2020, An alkaline lake in the Late Paleozoic Ice Age (LPIA): A review and new insights into paleoenvironment and petroleum geology: Earth-Science Reviews, **202**, 103091, doi: 10.1016/j.earscirev.2020.103091.

Cao, J., S. Yao, Z. Jin, W. Hu, Y. Zhang, X. Wang, Y. Zhang, and Y. Tang, 2006, Petroleum migration and mixing in the northwestern Junggar Basin (NW China): Constraints from oil-bearing fluid inclusion analyses: Organic Geochemistry, **37**, 827–846, doi: 10.1016/j.orggeochem.2006.02.003.

Chen, J., X. Pang, X. Wang, and Y. Wang, 2020, A new method for assessing tight oil, with application to the Lucaogou Formation in the Jimusaer depression, Junggar Basin, China: AAPG Bulletin, **104**, 1199–1229, doi: 10.1306/12191917401.

Chen, Z., T. Wang, Q. Liu, S. Zhang, and L. Zhang, 2015, Quantitative evaluation of potential organic-matter porosity and hydrocarbon generation and expulsion from mudstone in continental lake basins: A case study of Dongying sag, eastern China: Marine and Petroleum Geology, **66**, 906–924, doi: 10.1016/j.marpetgeo.2015.07.027.

Cortazar, G., and E. S. Schwartz, 1998, Monte Carlo evaluation model of an undeveloped oil field: Journal of Energy Finance Development, **3**, 73–84, doi: 10.1016/S1085-7443(99)80069-6.

Feng, C., T. Li, W. He, and M. Zheng, 2020, Organic geochemical traits and paleo-depositional conditions of source rocks from the Carboniferous to Permian sediments of the Northern Mahu Sag, Junggar Basin, China: Journal of Petroleum Science and Engineering, **191**, 107117, doi: 10.1016/j.petrol.2020.107117.

Guo, P., H. Wen, L. Gibert, J. Jin, Y. Jiang, and G. Wang, 2021, Controlling factors of high-quality hydrocarbon source rocks developed in lacustrine shallow-water zone of the Junggar Basin, northwestern China: AAPG Bulletin, **105**, 2063–2092, doi: 10.1306/03122119013.

Hackley, P. C., C. V. Araujo, A. G. Borrego, A. Bouzinos, B. J. Cardott, A. C. Cook, C. Eble, D. Flores, T. Gentzis, P. A. Gonçalves, J. G. Mendonça Filho, M. Hámor-Vidó, I. Jelonek, K. Kommeren, W. Knowles, J. Kus, M. Mastalerz, T. R. Menezes, J. Newman, I. K. Oikonomopoulos, M. Pawlewicz, W. Pickel, J. Potter, P. Ranasinghe, H. Read, J. Reyes, G. D. L. Rosa Rodriguez, I. V. Alves Fernandes de Souza, I. Suárez-Ruiz, I. Sýkorová, and B. J. Valentine, 2015, Standardization of reflectance measurements in dispersed organic matter: Results of an exercise to improve interlaboratory agreement: Marine and Petroleum Geology, **59**, 22–34, doi: 10.1016/j.marpetgeo.2014.07.015.

Hakimi, M. H., A. Ahmed, A. Y. Kahal, O. S. Hersi, H. J. Al Faifi, and S. Qaysi, 2020, Organic geochemistry and basin modeling of Late Cretaceous Harshiyat Formation in the onshore and offshore basins in Yemen: Implications for effective source rock potential and hydrocarbon generation: Marine and Petroleum Geology, **122**, 104701, doi: 10.1016/j.marpetgeo.2020.104701.

Hakimi, M. H., and A. F. Ahmed, 2016, Organic-geochemistry characterization of the Paleogene to Neogene source rocks in the Sayhut subbasin, Gulf of Aden Basin, with emphasis on organic-matter input and petroleum-generation potential: AAPG Bulletin, **100**, 1749–1774, doi: 10.1306/05241615201.

Hu, S., W. Zhao, L. Hou, Z. Yang, R. Zhu, S. Wu, B. Bai, and X. Jin, 2020, Development potential and technical strategy of continental shale oil in China: Petroleum Exploration and Development, **47**, 877–887, doi: 10.1016/S1876-3804(20)60103-3.

Hu, T., X. Pang, F. Jiang, C. Zhang, G. Wu, M. Hu, L. Jiang, Q. Wang, T. Xu, Y. Hu, S. Jiang, W. Wang, and M. Li, 2022b, Dynamic continuous hydrocarbon accumulation (DCHA): Existing theories and a new unified accumulation model: Earth-Science Reviews, **232**, 104109, doi: 10.1016/j.earscirev.2022.104109.

Hu, T., X. Pang, S. Jiang, Q. Wang, X. Zheng, X. Ding, Y. Zhao, C. Zhu, and H. Li, 2018, Oil content evaluation of lacustrine organic-rich shale with strong heterogeneity: A case study of the Middle Permian Lucaogou Formation in Jimusaer Sag, Junggar Basin, NW China: Fuel, **221**, 196–205, doi: 10.1016/j.fuel.2018.02.082.

Hu, T., X. Pang, T. Xu, C. Li, S. Jiang, Q. Wang, Y. Chen, H. Zhang, C. Huang, and S. Gong, 2022a, Identifying the key source rocks in heterogeneous saline lacustrine shales: Paleogene shales in the Dongpu depression, Bohai Bay Basin, eastern China: AAPG Bulletin, **106**, 1325–1356, doi: 10.1306/01202218109.

Hu, T., X. Q. Pang, F. J. Jiang, Q. F. Wang, X. H. Liu, Z. Wang, S. Jiang, G. Y. Wu, C. J. Li, T. W. Xu, M. W. Li, J. W. Yu, and C. X. Zhang, 2021b, Movable oil content evaluation of lacustrine organic-rich shales: Methods and a novel quantitative evaluation model: Earth-Science Reviews, **214**, 103545, doi: 10.1016/j.earscirev.2021.103545.

Hu, T., X.-Q. Pang, F.-J. Jiang, Q.-F. Wang, G.-Y. Wu, X.-H. Liu, S. Jiang, C.-R. Li, T.-W. Xu, and Y.-Y. Chen, 2021a, Key factors controlling shale oil enrichment in saline lacustrine rift basin: Implications from two shale oil wells in Dongpu Depression, Bohai Bay Basin: Petroleum Science, **18**, 1578–1588, doi: 10.1016/j.petsci.2021.08.013.

Huang, H., R. Li, W. Chen, L. Chen, Z. Jiang, F. Xiong, W. Guan, S. Zhang, and B. Tian, 2021, Revisiting movable fluid space in tight fine-grained reservoirs: A case study from Shahejie shale in the Bohai Bay Basin, NE China: Journal of Petroleum Science and Engineering, **207**, 109170, doi: 10.1016/j.petrol.2021.109170.

Huang, H., R. Li, Z. Jiang, J. Li, and L. Chen, 2020a, Investigation of variation in shale gas adsorption capacity with burial depth: Insights from the adsorption potential theory: Journal of Natural Gas Science and Engineering, **73**, 103043, doi: 10.1016/j.jngse.2019.103043.

Huang, H., R. Li, F. Xiong, H. Hu, W. Sun, Z. Jiang, L. Chen, and L. Wu, 2020b, A method to probe the pore-throat structure of tight reservoirs based on low-field NMR: Insights from a cylindrical pore model: Marine and Petroleum Geology, **117**, 104344, doi: 10.1016/j.marpetgeo.2020.104344.

Huang, W. B., O. Salad Hersi, S. F. Lu, and S. W. Deng, 2017, Quantitative modelling of hydrocarbon expulsion and quality grading of tight oil lacustrine source rocks: Case study of Qingshankou 1 member, central depression, Southern Songliao Basin, China: Marine and Petroleum Geology, **84**, 34–48, doi: 10.1016/j.marpetgeo.2017.03.021.

Imin, A., M. Zha, X. Ding, B. Bian, Y. Liu, M. Zheng, and C. Han, 2020, Identification of a Permian foreland basin in the western Junggar Basin (NW China) and its impact on hydrocarbon accumulation: Journal of Petroleum Science and Engineering, **187**, 106810, doi: 10.1016/j.petrol.2019.106810.

Jarvie, D. M., 2012, Shale resource systems for oil and gas part 2: Shale-oil resource systems, *in* J. A. Breyer, ed., Shale reservoirs — Giant resources for the 21st Century: AAPG Memoir, **97**, 89–119.

Jarvie, D. M., R. J. Hill, T. E. Ruble, and R. M. Pollastro, 2007, Unconventional shale-gas systems: The Mississippian Barnett Shale of north-central Texas as one model for thermogenic shale-gas assessment: AAPG Bulletin, **91**, 475–499, doi: 10.1306/12190606068.

Jin, Z., X. Liang, and Z. Bai, 2022, Exploration breakthrough and its significance of Gulong lacustrine shale oil in the Songliao Basin, Northeastern China: Energy Geoscience, **3**, 120–125, doi: 10.1016/j.engeos.2022.01.005.

Katz, B., and F. Lin, 2014, Lacustrine basin unconventional resource plays: Key differences: Marine and Petroleum Geology, **56**, 255–265, doi: 10.1016/j.marpetgeo.2014.02.013.

Katz, B. J., and F. Lin, 2021, Consideration of the limitations of thermal maturity with respect to vitrinite reflectance, T_{max}, and other proxies: AAPG Bulletin, **105**, 695–720, doi: 10.1306/09242019261.

Li, M., Z. Chen, X. Ma, T. Cao, M. Qian, Q. Jiang, G. Tao, Z. Li, and G. Song, 2019, Shale oil resource potential and oil mobility characteristics of the Eocene-Oligocene Shahejie Formation, Jiyang Super-Depression, Bohai Bay Basin of China: International Journal of Coal Geology, **204**, 130–143, doi: 10.1016/j.coal.2019.01.013.

Liang, C., Y. Cao, Z. Jiang, J. Wu, S. Guoqi, and Y. Wang, 2017, Shale oil potential of lacustrine black shale in the Eocene Dongying depression: Implications for geochemistry and reservoir characteristics: AAPG Bulletin, **101**, 1835–1858, doi: 10.1306/01251715249.

Liu, B., E. Jia, Y. Lv, Q. Chang, C. Dai, and M. Li, 2014, Parameters and method for shale oil assessment: Taking Qinshankou Formation shale oil of Northern Songliao Basin: Journal of Central South University, **45**, 3846–3852.

Liu, G., Z. Chen, X. Wang, G. Gao, B. Xiang, J. Ren, and W. Ma, 2016, Migration and accumulation of crude oils from Permian lacustrine source rocks to Triassic reservoirs in the Mahu depression of Junggar Basin, NW China: Constraints from pyrrolic nitrogen compounds and fluid inclusion analysis: Organic Geochemistry, **101**, 82–98, doi: 10.1016/j.orggeochem.2016.08.013.

Michael, G. E., J. Packwood, and A. Holba, 2013, Determination of in-situ hydrocarbon volumes in liquid rich shale plays: Unconventional Resources Technology Conference, SEG, Global Meeting Abstracts, doi: 10.1190/urtec2013-211.

Milliken, K. L., T. Zhang, J. Chen, and Y. Ni, 2021, Mineral diagenetic control of expulsion efficiency in organic-rich mudrocks, Bakken Formation (Devonian-Mississippian), Williston Basin, North Dakota, U.S.A: Marine and Petroleum Geology, **127**, 104869, doi: 10.1016/j.marpetgeo.2020.104869.

Pang, X., M. Li, S. Li, and Z. Jin, 2005, Geochemistry of petroleum systems in the Niuzhuang South Slope of Bohai Bay Basin: Part 3. Estimating hydrocarbon expulsion from the Shahejie formation: Organic Geochemistry, **36**, 497–510, doi: 10.1016/j.orggeochem.2004.12.001.

Romero-Sarmiento, M.-F., M. Ducros, B. Carpentier, F. Lorant, M.-C. Cacas, S. Pegaz-Fiornet, S. Wolf, S. Rohais, and I. Moretti, 2013, Quantitative evaluation of TOC, organic porosity and gas retention distribution in a gas shale play using petroleum system modeling: Application to the Mississippian Barnett Shale: Marine and Petroleum Geology, **45**, 315–330, doi: 10.1016/j.marpetgeo.2013.04.003.

Tang, W., Y. Zhang, G. Pe-Piper, D. J. W. Piper, Z. Guo, and W. Li, 2021a, Permian to early Triassic tectono-sedimentary evolution of the Mahu sag, Junggar Basin, western China: Sedimentological implications of the transition from rifting to tectonic inversion: Marine and Petroleum Geology, **123**, 104730, doi: 10.1016/j.marpetgeo.2020.104730.

Tang, Y., J. Cao, W.-J. He, X.-G. Guo, K.-B. Zhao, and W.-W. Li, 2021b, Discovery of shale oil in alkaline lacustrine basins: The Late Paleozoic Fengcheng Formation, Mahu Sag, Junggar Basin, China: Petroleum Science, **18**, 1281–1293, doi: 10.1016/j.petsci.2021.04.001.

Tao, K., J. Cao, X. Chen, Z. Nueraili, W. Hu, and C. Shi, 2019, Deep hydrocarbons in the northwestern Junggar Basin (NW China): Geochemistry, origin, and implications for the oil vs. gas generation potential of post-mature saline lacustrine source rocks: Marine and Petroleum Geology, **109**, 623–640, doi: 10.1016/j.marpetgeo.2019.06.041.

Wang, M., R. W. T. Wilkins, G. Song, L. Zhang, X. Xu, Z. Li, and G. Chen, 2015, Geochemical and geological characteristics of the Es3L lacustrine shale in the Bonan sag, Bohai Bay Basin, China: International Journal of Coal Geology, **138**, 16–29, doi: 10.1016/j.coal.2014.12.007.

Wendebourg, J., M. Blaizot, and F. Baudin, 2017, Worldwide shale-oil reserves: Towards a global approach based on the principles of petroleum system and the petroleum system yield: Bulletin de la Société géologique de France, **188**, E4, doi: 10.1051/bsgf/2017201.

Wu, M., J. Cao, X. L. Wang, Y. Tang, B. Wang, B. L. Xiang, S. F. Kang, and W. F. Lan, 2014, Hydrocarbon generation potential of Triassic mudstones in the Junggar Basin, northwest China: AAPG Bulletin, **98**, 1885–1906, doi: 10.1306/03111413022.

Wu, Y., C. Liu, F. Jiang, T. Hu, R. S. Awan, Z. Chen, J. Lv, C. Zhang, M. Hu, R. Huang, and G. Wu, 2022a, Occurrence space and state of petroleum in Lacustrine Shale: Insights from two-step pyrolysis and the N_2 adsorption experiment: Energy & Fuels, **36**, 10920–10933, doi: 10.1021/acs.energyfuels.2c02222.

Wu, Y., C. Liu, F. Jiang, T. Hu, J. Lv, C. Zhang, X. Guo, L. Huang, M. Hu, R. Huang, R. S. Awan, and Y. Zhao, 2022b, Geological characteristics and shale oil potential of alkaline lacustrine source rock in Fengcheng Formation of the Mahu Sag, Junggar Basin, Western China: Journal of Petroleum Science and Engineering, **216**, 110823, doi: 10.1016/j.petrol.2022.110823.

Xiang, B., E. Li, X. Gao, M. Wang, Y. Wang, H. Xu, P. Huang, S. Yu, J. Liu, Y. Zou, and C. Pan, 2016, Petroleum generation kinetics for Permian lacustrine source rocks in the Junggar Basin, NW China: Organic Geochemistry, **98**, 1–17, doi: 10.1016/j.orggeochem.2016.05.003.

Xue, H., Z. Dong, S. Tian, S. Lu, H. C. Greenwell, P. Luo, W. Zhang, S. Lu, M. Wang, W. Ma, and Y. Wang, 2022, Calculation and controlled factors of hydrocarbon expulsion efficiency using corrected pyrolysis parameters: A Songliao case study: Journal of Petroleum Science and Engineering, **208**, 109026, doi: 10.1016/j.petrol.2021.109026.

Yang, Y., Y. Chen, Y. Qin, and Q. Cheng, 2008, Monte-Carlo method for coalbed methane resource assessment in key coal mining areas of China: Journal of China University of Geosciences, **19**, 429–435, doi: 10.1016/S1002-0705(08)60077-1.

Yu, K., Y. Cao, L. Qiu, and P. Sun, 2019, Depositional environments in an arid, closed basin and their implications for oil and gas exploration: The lower Permian Fengcheng Formation in the Junggar Basin, China: AAPG Bulletin, **103**, 2073–2115, doi: 10.1306/01301917414.

Zhang, H., H. Huang, Z. Li, and M. Liu, 2019, Oil physical status in lacustrine shale reservoirs — A case study on Eocene Shahejie Formation shales, Dongying Depression, East China: Fuel, **257**, 116027, doi: 10.1016/j.fuel.2019.116027.

Zheng, T., X. Ma, X. Pang, W. Wang, D. Zheng, Y. Huang, X. Wang, and K. Wang, 2019, Organic geochemistry of the Upper Triassic Tx source rocks and the hydrocarbon generation and expulsion characteristics in Sichuan Basin, central China: Journal of Petroleum Science and Engineering, **173**, 1340–1354, doi: 10.1016/j.petrol.2018.10.070.

Biographies and photographs of the authors are not available.